Monte Carlo Simulations of Neutral Beam Injection into the TJ-II Helical-Axis Stellarator

A.Teubel, J. Guasp and M. Liniers

IPP 4/268

March 1994

MAX-PLANCK-INSTITUT FÜR PLASMAPHYSIK

85748 GARCHING BEI MÜNCHEN

MAX-PLANCK-INSTITUT FÜR PLASMAPHYSIK

GARCHING BEI MÜNCHEN

Monte Carlo Simulations of Neutral Beam Injection into the TJ-II Helical-Axis Stellarator

A.Teubel, J. Guasp and M. Liniers

IPP 4/268 March 1994

Die nachstehende Arbeit wurde im Rahmen des Vertrages zwischen dem Max-Planck-Institut für Plasmaphysik und der Europäischen Atomgemeinschaft über die Zusammenarbeit auf dem Gebiete der Plasmaphysik durchgeführt.

Monte Carlo Simulations of Neutral Beam Injection into the TJ-II Helical-Axis Stellarator

A. TEUBEL

Max-Planck-Institut für Plasmaphysik, IPP-EURATOM Association,
D-85748 Garching bei München, Germany

J. GUASP and M. LINIERS

Asociación EURATOM/CIEMAT para Fusión
28040 Madrid, Spain

Abstract — The neutral beam injection (NBI) efficiency for the TJ-II helical-axis stellarator was studied by Monte Carlo simulations for the case of tangential injection. For benchmark purposes, two different NBI codes are applied which take into account the peculiar geometries of the NBI, vacuum vessel, and helical-indented magnetic surfaces in TJ-II.

The results obtained for various plasma parameters are discussed, emphasis being placed on comparing the co- and counter-heating efficiencies and considering loss mechanisms. The results from the two codes are in good agreement if differences in the magnetic field configurations used are borne in mind.

The Monte Carlo code, which treats the guiding center part in magnetic coordinates, was used to investigate the influence of an assumed radial electric field on the heating efficiency. An interesting type of resonance which enhances fast orbit losses has been found for $\omega_{\mathrm{pol}}/\omega_{\mathrm{tor}} \approx 2$ (with ω_{pol} and ω_{tor} being the poloidal and toroidal frequencies of the fast ions, respectively). This critical ratio can be reached during slowing-down owing to the $\vec{E} \times \vec{B}$ -drift.

1. INTRODUCTION

The TJ-II device is a medium-size helical-axis stellarator to be built at CIEMAT in Madrid (TJ-II GROUP, 1990) (Table 1). Its main characteristics are potential for high-beta operation, variation of the rotational transform over a wide range, and bean-shaped plasma cross-section.

After a first experimental stage with electron cyclotron resonance heating (400 kW at 53.2 GHz, the second harmonic in X-mode), neutral beam injection (NBI) heating is planned in two steps: the first one with two tangential injectors (co and counter, each with 1 MW) and the second with up to 4 MW of injected power, including quasi-perpendicular injection (beams 5 and 6 in Fig. 1).

First NBI simulations with the FAFTJ1 code were mainly devoted to optimising the beam geometry and beam energy with respect to the heating efficiency (GUASP and LINIERS, 1993A and 1993B). Due to unexpected results in the form of strong peaking of the heating profile a benchmark with a second code (FAFTJ2) was performed. Additionally, FAFTJ2 allows electric field effects to be studied much more easily. A radial electric field E_{rad} has less influence on fast ion confinement with tangential injection than with perpendicular injection, as is known from simulations for other stellarators (FOWLER et. al., 1990 and 1991; HANATANI and PENNINGSFELD, 1992; TEUBEL and PENNINGSFELD, 1992, 1993A, and 1993B). Nevertheless, it is worthwhile to investigate this effect for tangential injection into TJ-II, too, as a first step toward studies for the planned perpendicular injection.

The following convention is chosen here: Co-injection is associated with an increasing rotational transform due to beam-driven current. Thus, for the right-handed TJ-II $v_{||} := \vec{v}\vec{B}/B > 0$ coincides with the co-direction, in contrast to the W7 family.

2. NBI MONTE CARLO CODES

The FAFNER code simulates the injection of fast neutral particles into a toroidal plasma and the orbits of resulting ions, including charge-exchange and re-ionisation processes. It allows evaluation of the global heating efficiency, the losses (scraper, shine-through, charge-exchange, and orbit losses, including those to limiters), the birth profile, and the heating profile. The field configuration, the E_{rad}-profile, plasma density and temperature profiles, as well as the beam parameters (e.g. divergence and focusing of the beam, scraper and source shapes, neutral species with its energy mixing) are taken as input parameters.

The FAFTJ1 and FAFTJ2 codes used in this work are adaptions and extensions of two versions (LISTER, 1985 and 1986) of the FAFNER fully three-dimensional code to the special geometries in TJ-II (NBI, coils, vacuum vessel, and helical-indented magnetic surfaces). In the absence of an electric field the two FAFNER codes applied to W7-AS were benchmarked. Results for calculated orbits as well as birth and heating profiles were found to be in good agreement (TEUBEL, 1993).

The main difference between FAFTJ1 and FAFTJ2 is the evaluation of guiding center orbits. The second treats this part in magnetic coordinates (toroidal magnetic flux Ψ, toroidal and poloidal angles Φ and Θ, respectively (BOOZER, 1980; KUO-PETRAVIC et. al., 1983) instead of real-space coordinates (R, ϕ, and z). Using "Boozer" coordinates has several advantages, the main ones being the separation of the slow motion across the field lines from the fast motion along the field lines and the natural representation of quantities which are constant on magnetic surfaces (e.g. the electric potential, densities, and temperatures).

The calculation and representation of the magnetic field input parameters are different in the two codes. For FAFTJ1 the B-field vector and the gradients as well as the average plasma radius and volume are generated by a field line code. These quantities are stored on a 3-D grid for each magnetic configuration. FAFTJ2 uses analytic representations of quantities necessary for guiding center calculations (modulus of B-field as a function of Ψ, Φ, and Θ, and the rotational transform, volume, and poloidal and toroidal currents as functions of Ψ) which are obtained from a MHD equilibrium code. An additional data set generated by these calculations allows transformation of real-space coordinates to "Boozer" coordinates and vice versa.

If guiding center orbits (GCO) are solved in "Boozer" coordinates, the plasma can only be described up to the last closed flux surface (LCFS). A particle is therefore assumed to be lost or to leave the plasma if the LCFS is crossed. The re-entry effect can be taken into account in FAFTJ1. There, a fast ion is followed without collisions if its effective radius exceeds a maximum value, which has to be set by the user. In this way the GCO can be followed outside the LCFS.

3. CHOICE OF INJECTION AND PLASMA PARAMETERS

The main input parameters of the NBI simulations are listed in Table 2. In previous calculations the FAFTJ1 code was used in combination with a one-dimensional transport code to include effects of density buildup and temperature evolution on the absorption of neutral power by the plasma, as well as to get a roughly consistent set of radial profiles and central values at different discharge times (GUASP and LINIERS, 1993A and 1993B). According to these evaluations, three different density-temperature scenarios (low, medium, and high density) are studied in this work. The following profile function for $T_{e,i}(r)$ and $n_e(r)$ is taken:

$$G(r) = (G(0) - G(a))(1 - (r/a)^{\alpha})^{\beta} + G(a) \quad ,$$

where r is the effective radius, and $G(0)$ and $G(a)$ are the values of the variable G on the plasma axis and at the minor plasma radius a.

To simplify matters, only one standard vacuum B-field configuration and one neutral gas density profile with exponential decay were taken. Furthermore, impurities were neglected.

The high density case was simulated with FAFTJ2 to investigate E_{rad} effects on the confinement. The potential, which is not self-consistent, was chosen in the form

$$V(\Psi) = V_0(1 - \Psi/\Psi_b) \quad .$$

Ψ_b specifies the LCFS with $(r/a)^2 = \Psi/\Psi_b$. The potential strength varies in a range $|V_0| < 5$ kV. As known from other experiments, a positive potential V_0 can generally be excluded in the confinement region – nevertheless these results are also presented for completeness.

4. COMPARISON OF RESULTS

4.1 Shine-through and Birth Profile

The algorithms for tracing the neutrals to the plasma edge are nearly identical in the two codes. The errors due to statistical noise are less than 0.1% for the calculated scraper losses of 10%.

Small differences in shine-through losses (Fig. 2a) are mainly due to the magnetic field structures used in the two codes being not identical. The effective radii determined for real space points are larger for FAFTJ1 than for FAFTJ2, especially near the plasma boundary ($\Delta r_{1-2} \approx 2$ cm). This can be seen by determining the effective radii of a neutral following a path along the beamline axis or by comparing flux surfaces.

The NBI geometry in TJ-II is point-symmetric for co- and counter-beams. Co- and counter-birth profiles, which have to be identical, are in good agreement for the simulations within the statistical errors. Near the magnetic axis the error bars of the power density are of course larger due to the smaller volume element. More neutrals were followed in FAFTJ2 (9,000 per source) and a larger cone width was chosen than in FAFTJ1 (3,000 per source). Therefore, the FAFTJ2 birth profiles are "smoother" (Fig. 2b). The profiles clearly show the stronger penetration of neutrals into the plasma at lower densities.

4.2 Losses, heating efficiency and profiles

Mainly the pitch angle distribution of fast ions when born determines the topology of collisionless orbits. An ion starting in a toroidal plane Φ with pitch $|\zeta| = |v_{||}/v| > \sqrt{1 - B_{\mathrm{min}}(\Phi)/B_{\mathrm{max}}} = |\zeta(\Phi)|_{\mathrm{crit}}$ cannot be reflected according to the adiabatic invariance of the magnetic moment. Due to the nearly tangential injection into TJ-II ($|\zeta|_{\mathrm{inj}} > 0.8$) all ions start as passing particles (Fig. 3). Such particles can be lost after few poloidal rotations in a time (typically $< 10^{-4}$ s) independent of the plasma temperature and density. This is the main orbit loss mechanism for TJ-II tangential injection without an electric field. To study this effect, it is useful to determine the "maximum guiding center" (MGCO) of passing particles, defined as follows: For a given pitch angle and energy, the starting point (Ψ, Φ, Θ) of an ion is shifted outward until the resulting collisionless GCO reaches Ψ_b. Particles starting outside the MGCO are lost. The MGCO are relatively independent

of the pitch for $|\zeta| > 0.6$. Below this value the MGCO are very sensitive to changes in $|\zeta|$ (Fig. 4). Poincaré plots of collisionless passing orbits in TJ-II are characterised by strong variation (compared with W7-AS) with the toroidal angle (Fig. 4 and 5).

The global heating efficiency η_h depends on various mechanisms: shine-through, charge-exchange, and orbit losses. The main parameter is the electron density. At high densities more ions are born in the outer region and prompt orbit losses increase. The higher orbit losses for co-injection than for counter-injection can be explained by the remarkable variation of drift orbits with the toroidal angle Φ. It is interesting to note that this behavior is different to the situation in tokamaks and, for example, W7-AS, where co-injection is more efficient. In the low-density region η_h is mainly limited by shine-through losses. Additionally, a higher probability of charge-exchange processes due to the increased slowing-down time decreases the efficiency. Comparison of FAFTJ1 and FAFTJ2 results indicates good agreement, especially for the medium- and low-density scenarios (Fig. 6). A similar situation appears if both codes are compared for a slightly different NBI geometry and with full particle energy $E_0 = 40$ keV (Fig. 7). At high densities differences in the magnetic field configurations used are more important, due to the high sensitivity of prompt orbit losses to the birth position near the plasma edge. The influence of re-entering has been studied in FAFTJ1 and found to be largely independent of density and amounting to less than 10% in η_h.

According to the different electron temperatures of the low-, medium-, and high-density cases the ratios of ion to electron heating are about 1:1, 3:4, and 1:2, respectively.

The heating profiles show the expected behavior with respect to density dependence. The profiles determined by FAFTJ1 and FAFTJ2 are comparable taking into account the different magnetic field configurations and statistical noise (Fig. 8). Co- and counter-profiles are not shifted inward and outward (Fig. 9), respectively, as for W7-AS or tokamak injection. The strong peaking found in previous calculations could be identified as a numerical error in solving the differential equation of GCO. This problem was solved by decreasing the time step width and by using a finer grid for magnetic field representation. Now, collisionless orbits of passing particles agree quite well, within expected differences due to the different B-field configuration.

5. ELECTRIC FIELD EFFECTS

Another orbit loss mechanism plays a more important role if the electric field is taken into account. The rotational transform for the TJ-II configuration considered is high. E_{rad} can enhance the toroidal rotation up to the resonance condition $\omega_{pol}/\omega_{tor} = 2$. Near this resonance the topology of collisionless orbits changes. Co-particles are lost below and counter-particles above the resonance. A fast ion can approach this region at fixed potential V_0 owing to energy decrease during slowing-down (Fig. 10). The toroidal resonance $\omega_{pol} = 0$ known from W7-A and W7-AS (HANATANI and PENNINGSFELD, 1992; TEUBEL and PENNINGSFELD 1993B) is not important in TJ-II due to the higher rotational transform.

The influence of E_{rad} on η_h was studied for the high-density case, where orbit losses dominate. The increase of orbit losses for co-injection below a negative potential threshold

and for counter-injection above a positive potential threshold (Fig. 11a) can be understood in terms of the resonance effect. Charge-exchange losses depend weakly on V_0 (between 10% and 20%). Ions can gain or lose kinetic energy by radial motion from one magnetic surface to another with different electric potentials. Therefore, the strong increase of orbit losses is partly compensated in the heating efficiency for the counter case (Fig. 11b).

6. CONCLUSIONS

The benchmark studies of the two codes were successful. In the low- and medium-density cases our results agree very well. At high densities orbit losses are more sensitive to the magnetic field configurations near the edge. Differences in the calculated orbit losses are due to the different configurations used in FAFTJ1 and FAFTJ2.

According to the special TJ-II geometry the vacuum vessel can cross the LCFS determined by MHD calculations for FAFTJ2. In a next step it is planned to include this limiter effect, as has already been done in the FAFNER W7-AS version and clarify the role of re-entry effects in more detail with FAFTJ1. Extensive studies for optimisation of the NBI geometry and energy parameters are under way.

For perpendicular injection the E_{rad} effect plays a more important role. A first step toward understanding it was taken by our calculations of collisionless orbits of passing particles. The heating efficiency for tangential injection in TJ-II is affected by a positive (negative) potential in the counter- (co-) case, in contrast to W7-AS. The different resonance conditions for the two stellarators are given by $\omega_{\mathrm{pol}} = 2\omega_{\mathrm{tor}}$ and $\omega_{\mathrm{pol}} = 0$, respectively. A very helpful tool to understand E_{rad} effects for perpendicular injection are loss cones in velocity space. These are expected to depend very sensitively on the starting point chosen in TJ-II. Further studies are thus necessary.

ACKNOWLEDGEMENT

The authors acknowledge helpful discussions with F.-P. Penningsfeld, E. Speth, W. Ott, and J. Nührenberg of IPP and J. Jimenez of CIEMAT. The FAFTJ2 work was performed during a three-month stay of A.T. at CIEMAT supported by EURATOM.

REFERENCES

BOOZER A. H. (1980) *Physics Fluids* **23**, 904.

FOWLER R. H., MORRIS R. N., ROME A. R. and HANATANI K. (1990) *Nucl. Fusion* **30**, 997.

FOWLER R. H., MORRIS R. N., and ROME A. R. (1991) *Fusion Technol.* **20**, 200.

GUASP J. and LINIERS M. (1993A) *Fusion Technol.*, November.

GUASP J. and LINIERS M. (1993B) *Proc. 20th Europ. Conf. on Controlled Fusion and Plasma Physics* (Lisbon), ECA, 17C, Part III, 933, EPS Geneva.

HANATANI K. and PENNINGSFELD F.-P. (1992) *Nucl. Fusion* **32**, 1769.

KUO-PETRAVIC G., BOOZER A. H., ROME J. A., and FOWLER R. H. (1983) *J. of Comput. Phys.* **51**, 261.

LISTER G. G. (1985) *IPP/Report 4/222*, Garching.

LISTER G. G. (1986) *Status/Report at IPP*, Garching.

TEUBEL A. (1994) *IPP/Report 4/266*, Garching.

TEUBEL A. and PENNINGSFELD F.-P. (1992) *Proc. 19th Europ. Conf. on Controlled Fusion and Plasma Physics* (Innsbruck), ECA, 16C, Part I, 537, EPS Geneva.

TEUBEL A. and PENNINGSFELD F.-P. (1993A) *Proc. 20th Europ. Conf. on Controlled Fusion and Plasma Physics* (Lisbon), ECA, 17C, Part I, 401, EPS Geneva.

TEUBEL A. and PENNINGSFELD F.-P. (1993B) to appear in: *Plasma Physics and Controlled Fusion.*

TJ-II GROUP (1990) *Fusion Technol.* **17**, 200.

TABLE 1. MAIN PARAMETERS OF TJ-II

Design parameters		
Major radius [m]	R_0	1.5
Magnetic field [T]	B_0	1
Number of periods	m	4
Range of plasma radius [m]	a	0.10 to 0.20
Range of rotational transform	ι	0.96 to 2.50
Range of shear [%]		-1 to + 10
Range of magnetic well depth [%]		0 to 6

TABLE 2. PARAMETERS OF THE COMPUTATION FOR TJ-II

TJ-II		
Major radius [m]	R_0	1.5
Minor radius [m]	a	0.19
Magnetic field [T]	B_0	1
Rotational transform	$\iota(0)$	1.5
Ratio of thermal to magnetic energy [%]	$\langle\beta\rangle$	0
Beam		
Injected power per source [MW]	$P_{\rm inj}$	1
Injection energy [keV]	E_0	27
Power ratio of E_0, $E_0/2$, $E_0/3$ species	$\gamma^{(1)} : \gamma^{(2)} : \gamma^{(3)}$	0.67 : 0.22 : 0.11
Target plasma		
Effective charge of ions	$Z_{\rm eff}$	1
Neutral gas density [m^{-3}]	$n_0(a)$, $n_0(0)$	$1 \cdot 10^{17}$, $5 \cdot 10^{14}$

Low (L), medium (M), and high (H) density cases

		L	M	H
Electron density [$10^{20} m^{-3}$]	$n_e(0)$	0.19	0.58	1.11
Line averaged n_e [$10^{20} m^{-2}$]	$\bar{n}_e$	0.05	0.15	0.27
Electron temperature [eV]	$T_e(0)$	980	630	480
Ion temperature [eV]	$T_i(0)$	230	420	380

FIGURE CAPTIONS

FIG. 1. NBI geometry in TJ-II: four tangential beams (1 to 4) and two quasi-perpendicular beams (5 and 6).

FIG. 2. FAFTJ1-FAFTJ2 comparison of a) shine-through losses and b) birth profiles for the low (L), medium (M), and high (H) density cases with 2 MW injection.

FIG. 3. Pitch distribution of 1,000 born ions in the low-density case and critical pitch $|\zeta|_{\text{crit}}$ as a function of the toroidal angle.

FIG. 4. Poincaré plots (in $\sqrt{\Psi/\Psi_b}$, Θ-plane at toroidal angles Φ) of maximum guiding center orbits for different pitches in "Boozer" coordinates. Ions start at $\Phi_0 = 0$ and $\Theta_0 = 0$ with energy $E_0 = 27$ keV.

FIG. 5. Poincaré plots (at four toroidal angles ϕ) of drift surfaces (crosses) in real space coordinates for a co-and a counter-particle with energy $E_0 = 27$ keV and pitch $|\zeta| = 1$. The shown flux surfaces (dots) correspond to the starting position $R_0 =$ 150cm $+a/2$, $z_0 = 0$, and $\phi_0 = 0$ of the ions.

FIG. 6. Comparison of FAFTJ1 and FAFTJ2 results: a) charge-exchange losses, b) orbit losses, and c) heating efficiency depending on the electron density $n_e(0)$.

FIG. 7. Comparison of FAFTJ1 and FAFTJ2 results for balanced injection at $E_0 = 27$ keV and $E_0 = 40$ keV.

FIG. 8. Heating profiles of 2 MW balanced injection calculated with FAFTJ1 (full symbols) and FAFTJ2 (hollow symbols) for the three density scenarios.

FIG. 9. Heating profiles (co and counter, each with 1 MW for the three density scenarios (FAFTJ2 results).

FIG. 10. Poincaré plots (in $\sqrt{\Psi/\Psi_b}$, Θ-plane at toroidal angle $\Phi = 0$) of collisionless orbits for a) co-particles ($\Psi_0/\Psi_b = 0.25$, $V_0 = -3$ keV and $\zeta = +0.85$) and b) counter-particles ($\Psi_0/\Psi_b = 0.49$, $V_0 = +5$ keV, and $\zeta = -0.85$) starting at $\Phi_0 = 0$ and $\Theta_0 = 0$.

FIG. 11. a) Orbit losses and b) heating efficiency as a function of the electric potential in the high-density case.

Fig. 1

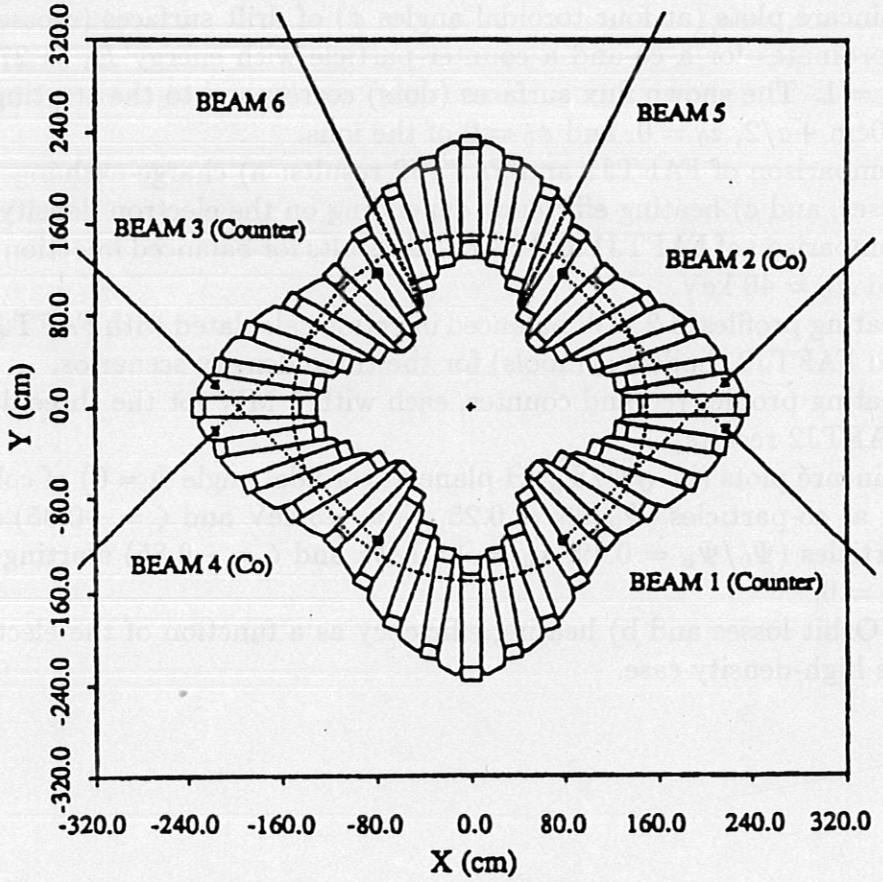
BEAM 6
BEAM 5
BEAM 3 (Counter)
BEAM 2 (Co)
BEAM 4 (Co)
BEAM 1 (Counter)
Y (cm)
X (cm)
320.0
240.0
160.0
80.0
0.0
-80.0
-160.0
-240.0
-320.0

Fig. 2

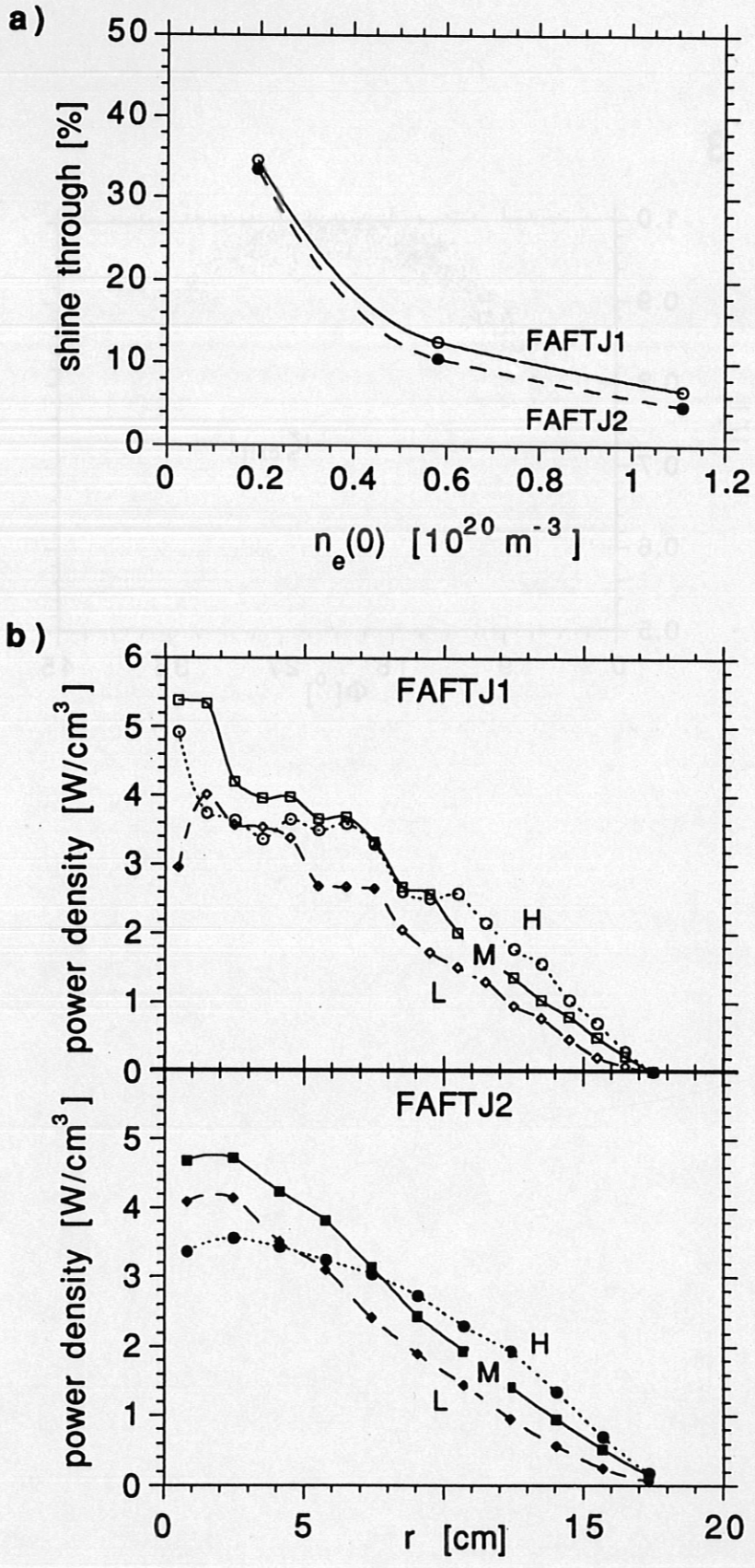
a)
shine through [%]
50
40
30
20
10
0
0
0.2
0.4
0.6
0.8
1
1.2
FAFTJ1
FAFTJ2
$n_e(0)$ [10^{20} m^{-3}]
b)
power density [W/cm^3]
FAFTJ1
H
M
L
FAFTJ2
H
M
L
0
5
15
20
r [cm]

Fig. 3

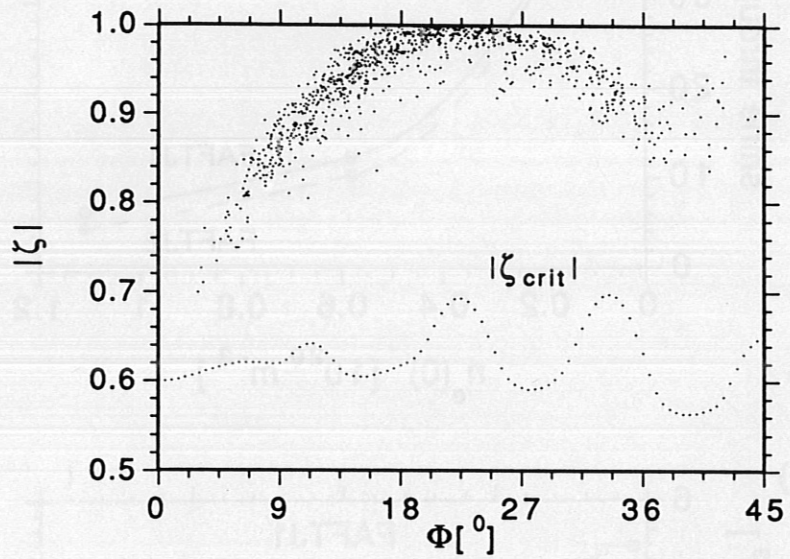

Fig. 4

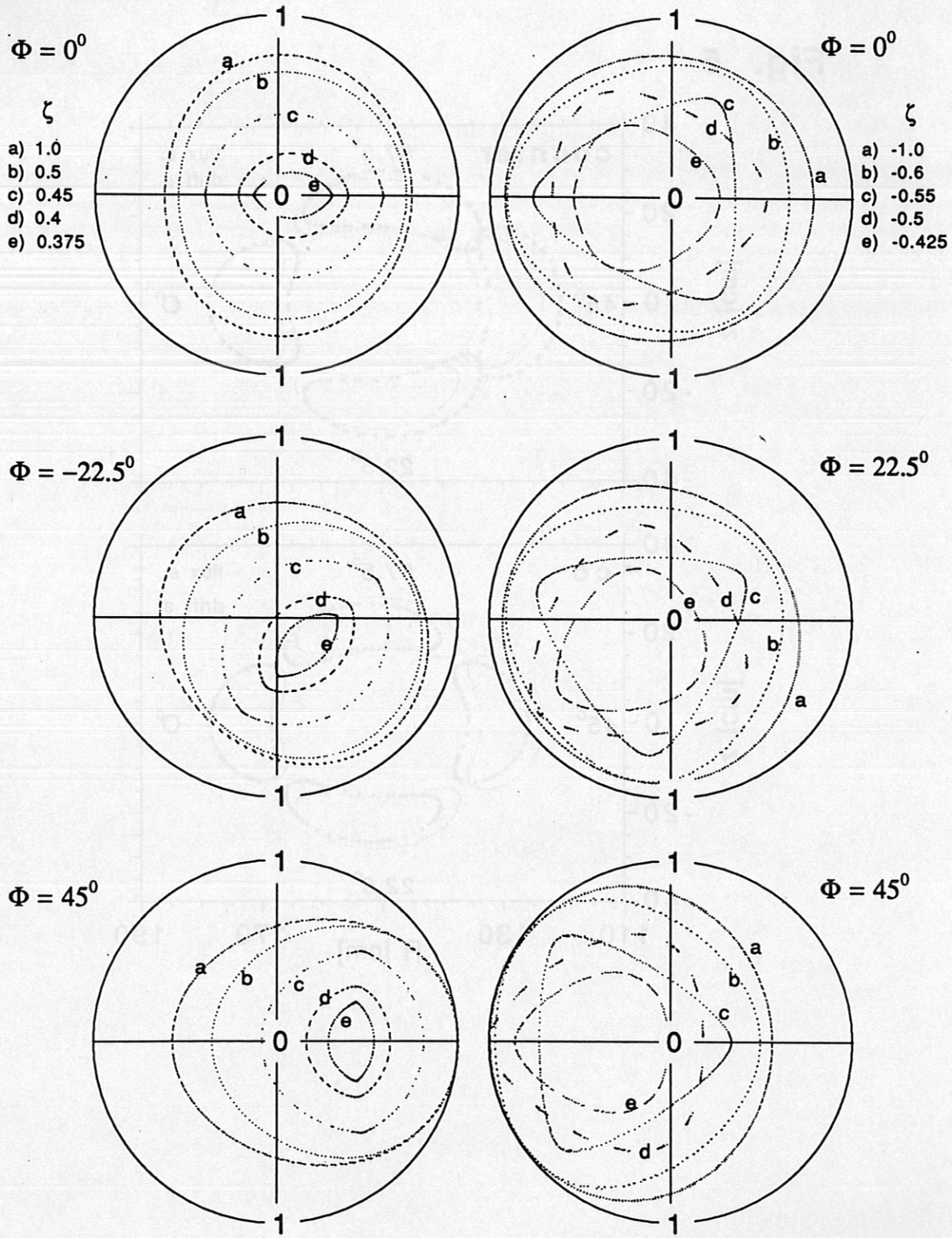
Φ = 0°
ζ
a) 1.0
b) 0.5
c) 0.45
d) 0.4
e) 0.375
Φ = 0°
ζ
a) -1.0
b) -0.6
c) -0.55
d) -0.5
e) -0.425
Φ = −22.5°
Φ = 22.5°
Φ = 45°
Φ = 45°
1
0
1

Fig. 5

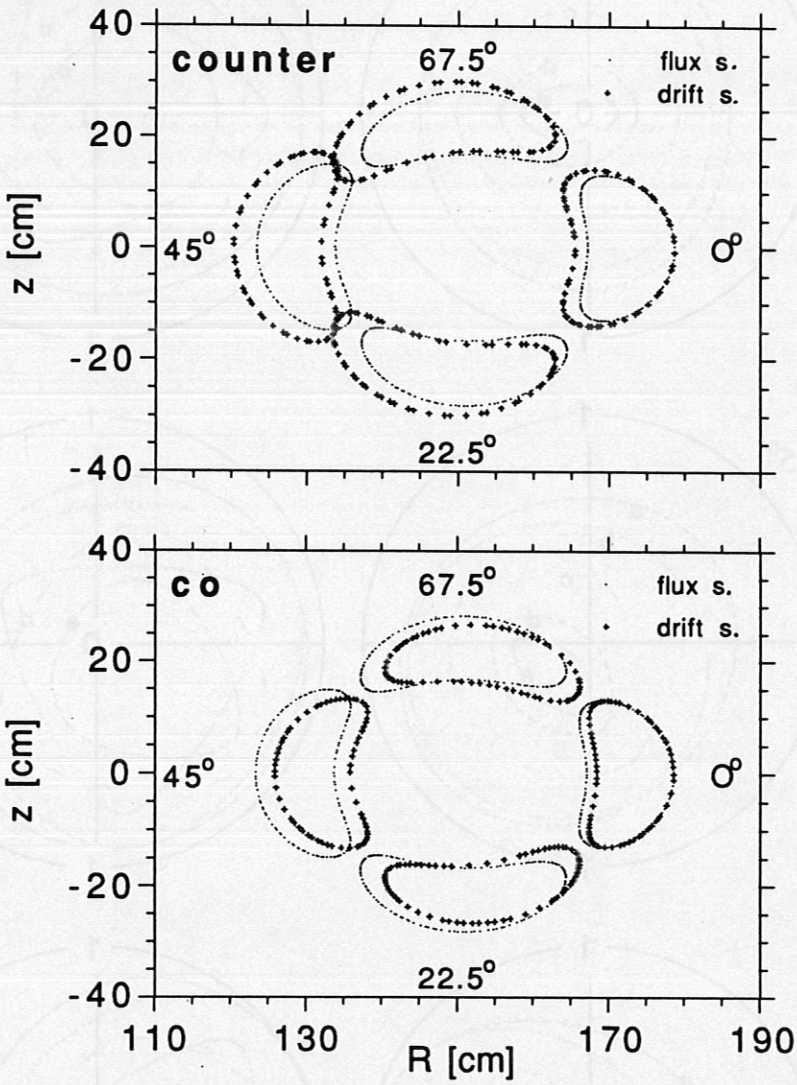
counter
67.5°
flux s.
drift s.
45°
0°
22.5°
co
67.5°
flux s.
drift s.
45°
0°
22.5°
z [cm]
40
20
0
-20
-40
110
130
170
190
R [cm]

Fig.6

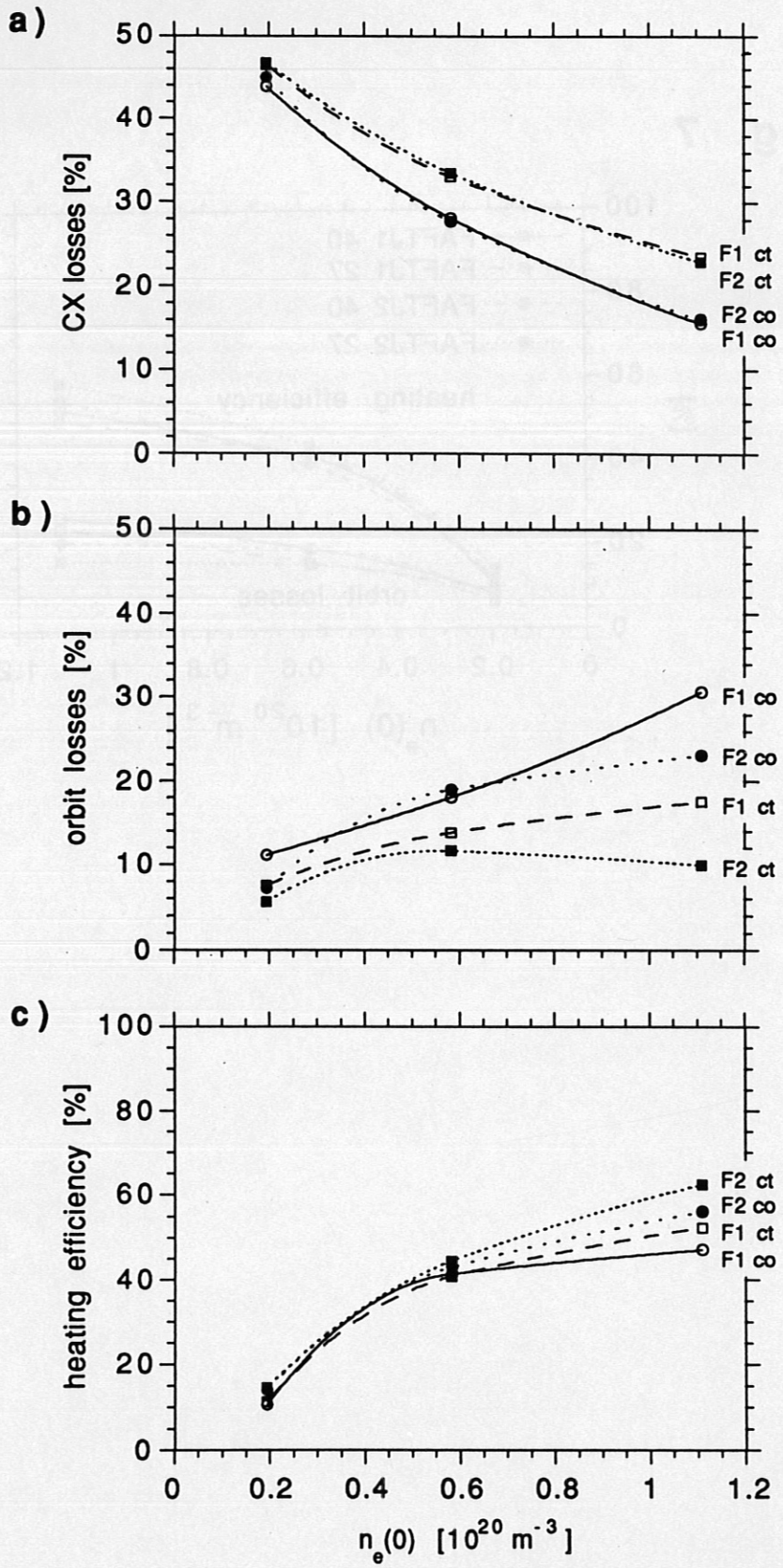
a)
CX losses [%]
50
40
30
20
10
0
F1 ct
F2 ct
F2 co
F1 co
b)
orbit losses [%]
50
40
30
20
10
0
F1 co
F2 co
F1 ct
F2 ct
c)
heating efficiency [%]
100
80
60
40
20
0
F2 ct
F2 co
F1 ct
F1 co
0
0.2
0.4
0.6
0.8
1
1.2
$n_e(0)$ [10^{20} m^{-3}]

Fig. 7

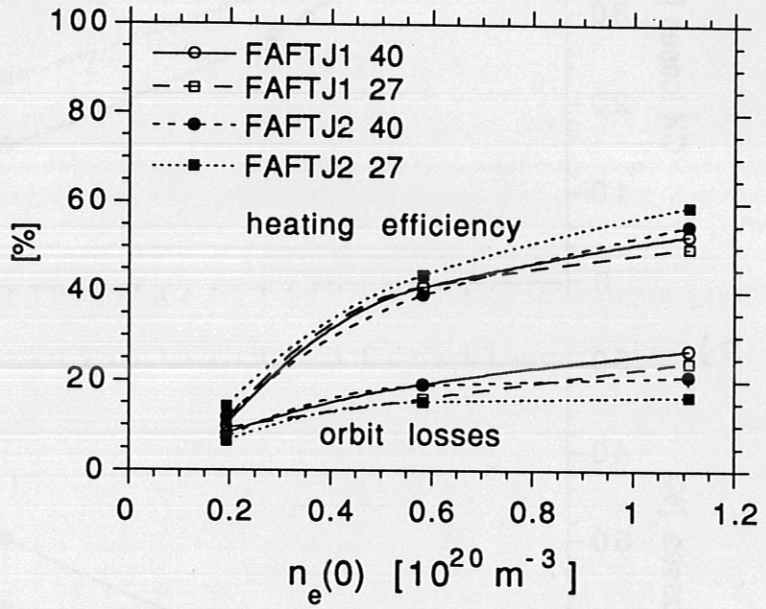
100
80
60
40
20
0
[%]
FAFTJ1 40
FAFTJ1 27
FAFTJ2 40
FAFTJ2 27
heating efficiency
orbit losses
0
0.2
0.4
0.6
0.8
1
1.2
$n_e(0)$ [10^{20} m^{-3}]

Fig. 7

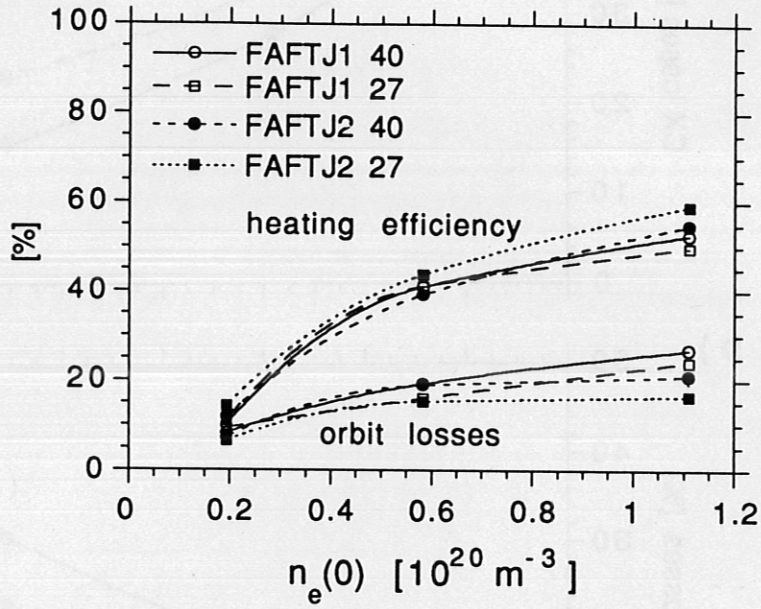
100
80
60
40
20
0
[%]
FAFTJ1 40
FAFTJ1 27
FAFTJ2 40
FAFTJ2 27
heating efficiency
orbit losses
0
0.2
0.4
0.6
0.8
1
1.2
$n_e(0)$ [10^{20} m^{-3}]

Fig. 8

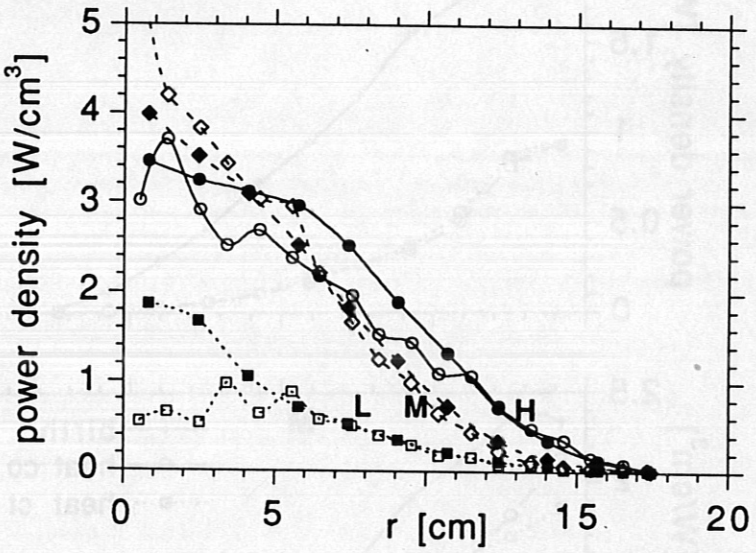

Fig. 9

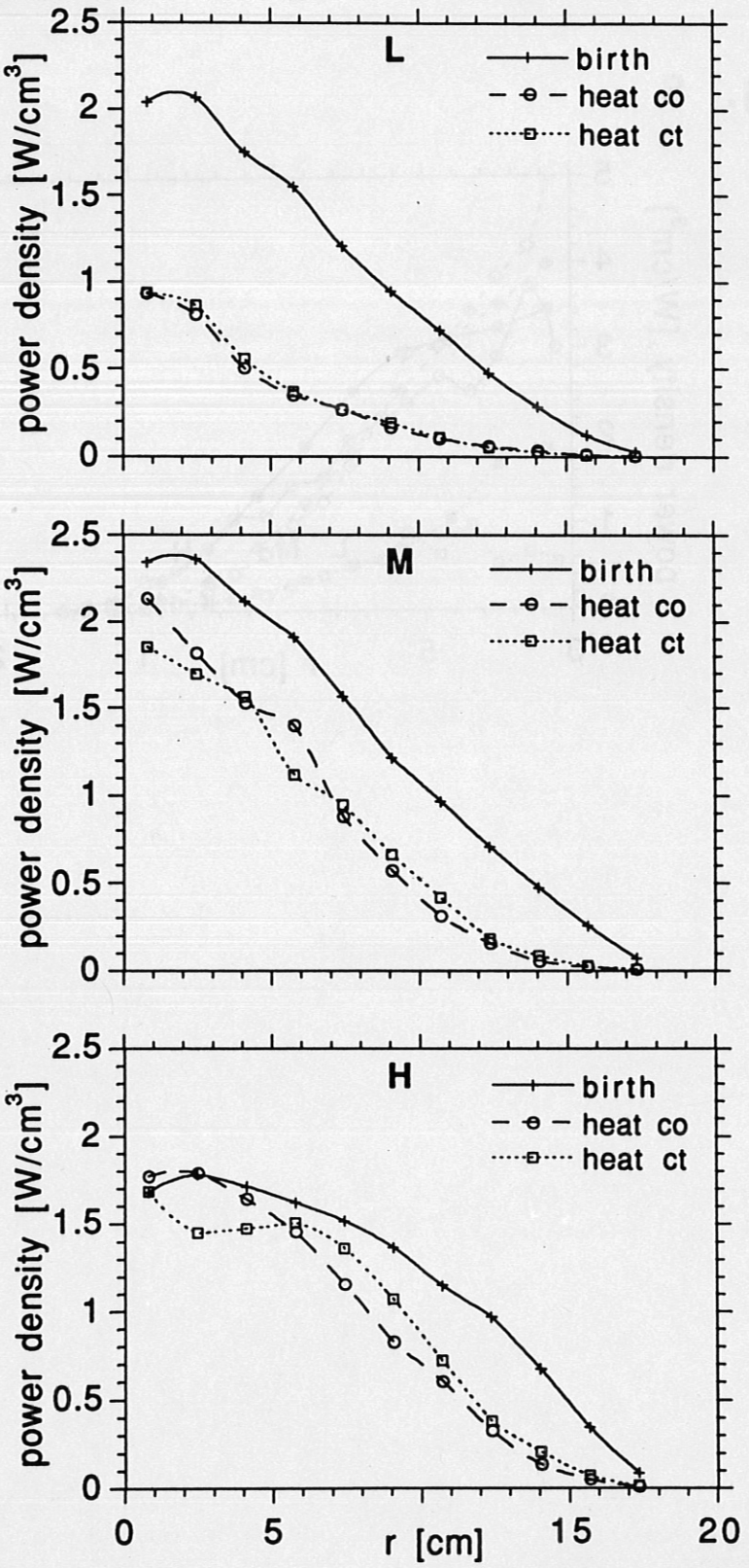
L
M
H
birth
heat co
heat ct
power density [W/cm^3]
r [cm]
0
0.5
1
1.5
2
2.5
5
15
20

Fig. 10

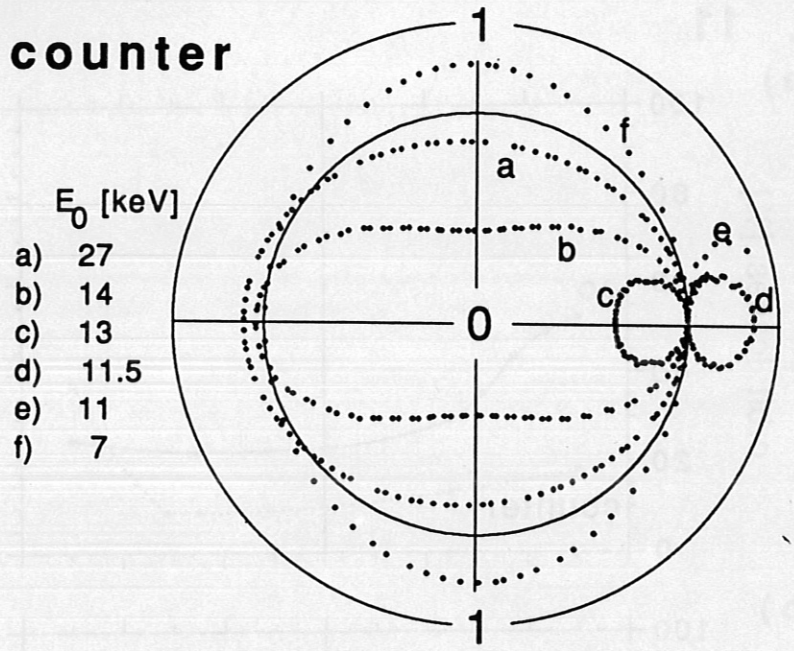
counter
E0 [keV]
a) 27
b) 14
c) 13
d) 11.5
e) 11
f) 7
1
0
1
a
b
c
d
e
f

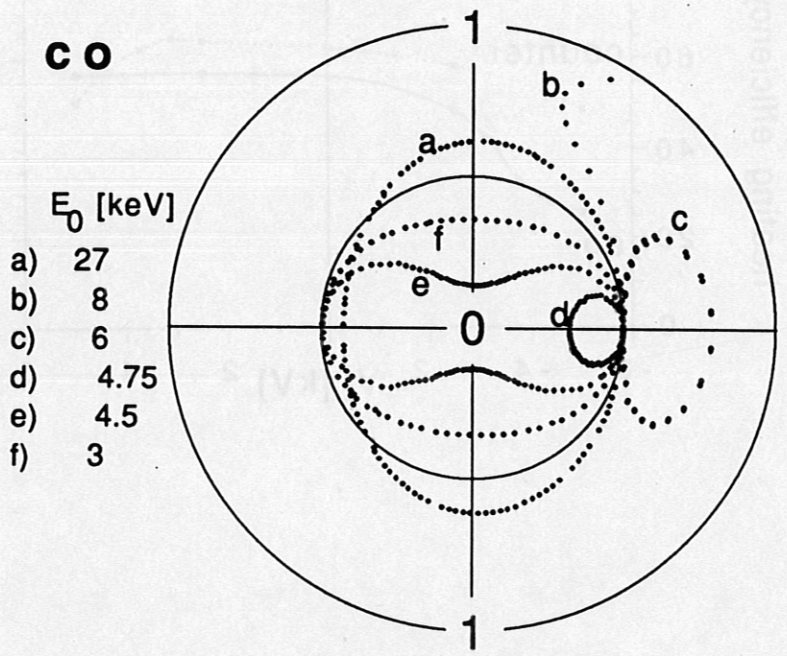
co
E0 [keV]
a) 27
b) 8
c) 6
d) 4.75
e) 4.5
f) 3
1
0
1
a
b
c
d
e
f

Fig. 11

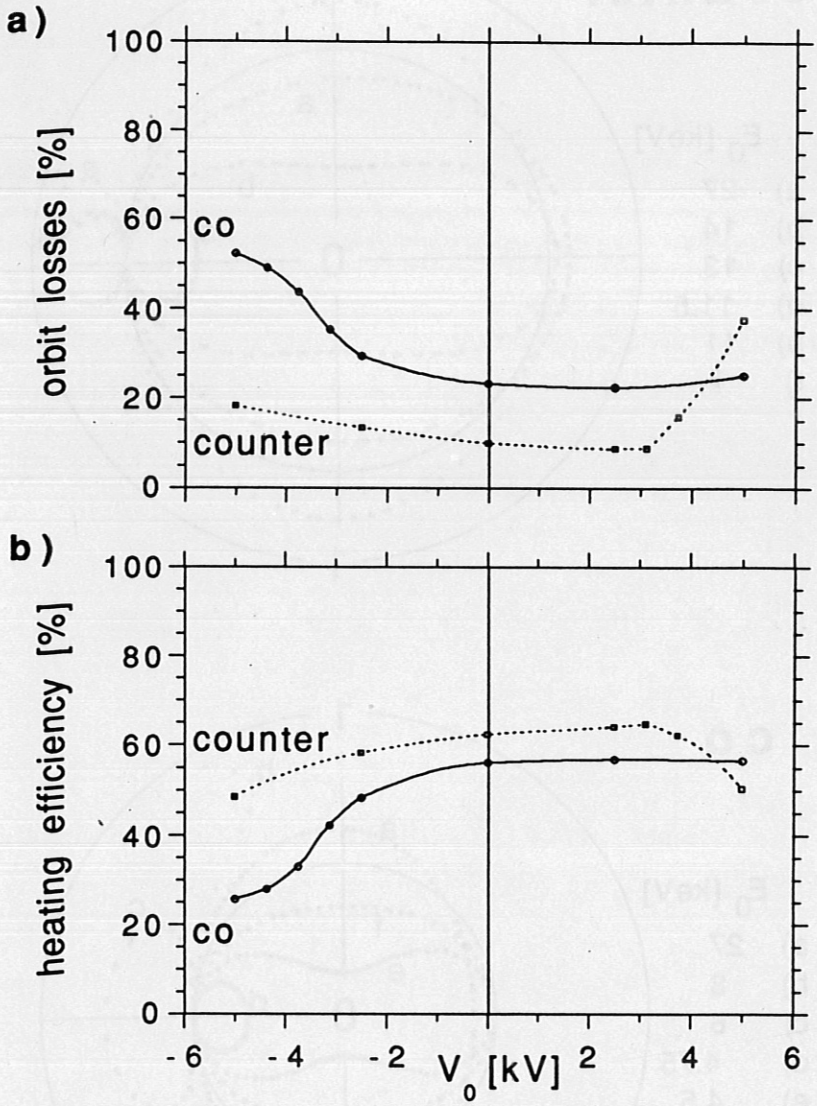
a)
orbit losses [%]
100
80
60
40
20
0
co
counter
b)
heating efficiency [%]
100
80
60
40
20
0
counter
co
-6
-4
-2
V0 [kV]
2
4
6